RAPID COMMUNICATIONS

PHYSICAL REVIEW B **91**, 081407(R) (2015)

Electrically tunable quantum spin Hall state in topological crystalline insulator thin films

Junwei Liu and Liang Fu

Department of Physics, Massachusetts Institute of Technology, Cambridge, Massachusetts 02139, USA

(Received 23 January 2015; published 27 February 2015)

Based on electronic structure calculations and theoretical analysis, we predict the (111) thin films of the SnTe class of three-dimensional (3D) topological crystalline insulators (TCIs) realize the quantum spin Hall phase in a wide range of thicknesses. The nontrivial topology originates from the intersurface coupling of the topological surface states of TCIs in the 3D limit. The intersurface coupling changes sign and gives rise to topological phase transitions as a function of film thickness. Furthermore, this coupling can be strongly affected by an external electric field, hence the quantum spin Hall phase can be effectively tuned under the experimentally accessible electric field.

DOI: 10.1103/PhysRevB.91.081407 PACS number(s): 73.21.−b, 73.43.−f, 73.61.−r

Topological crystalline insulators (TCIs) are topological phases of matter protected by crystal symmetries [1,2]. TCIs have attracted wide attention after the prediction and observation of this phase in IV-VI semiconductors SnTe, $Pb_{1-x}Sn_xSe$, and $Pb_{1-x}Sn_xTe$ [3–6]. The topological nature of the SnTe class of TCIs arises from the mirror symmetry of the rocksalt structure, and is manifested in the presence of topological surface states consisting of an even number of Dirac fermions. Recent experiments [7,8] have observed that two of the four Dirac fermions on the (001) surface become gapped when the structural distortion takes place and breaks one of the two mirror planes, as predicted by theory [3,9]. This observation establishes the topological protection by crystal symmetry—the defining property of TCIs.

There is currently an intensive experimental investigation of IV-VI TCIs in the low-dimensional and nanostructure form [10–17]. Recently we predicted that (001) films of TCIs with an odd number of atomic layers can possess spin-filtered gapless edge states. Interestingly, the edges states can be gapped by a perpendicular electric field that breaks the mirror symmetry. Based on this functionality, we proposed a topological transistor device in which spin and charge transport are coupled and can be simultaneously controlled by the electric field effect [18].

Due to the cubic structure in the bulk, electronic structures of IV-VI semiconductor thin films depend crucially on the growth direction [19–22]. In this Rapid Communication, we study (111) thin films of IV-VI TCIs, which have been grown epitaxially in recent experiments [11,15]. We find that (111) thin films can host the quantum spin Hall state [23–25] in a wide range of film thicknesses with both an even or odd number of layers (despite the different crystal symmetries in the two cases). The largest nontrivial gap is found to be around 50 meV. Here the quantum spin Hall phase arises from the coherent coupling between the top and bottom topological surface states of TCIs in the 3D limit. This intersurface coupling mechanism has been previously proposed in model studies of Bi_2Se_3 thin films [26–28], which inspired part of this work. Furthermore, we find that the intersurface coupling in (111) TCI thin films can be strongly tuned by a moderate external electric field, leading to an electrical control of the topological property.

For convenience, we will only show below the calculations for SnTe as a representative of TCIs in IV-VI semiconductors. All the qualitative conclusions apply to $Pb_{1-x}Sn_xTe$ and $Pb_{1-x}Sn_xSe$ as well. The rocksalt structure of SnTe has two inequivalent (111) surfaces, ending at a plane of Sn or Te atoms, respectively. Both surface states consist of four Dirac cones centered at time-reversal-invariant momenta: One is at the Γ point and the other three are at the M points [29–32], as observed in recent angle-resolved photoemission spectroscopy experiments [15,33,34]. Different from (001) surface states, these four Dirac cones here are not all equivalent. Specifically, the Dirac point at the Γ point is well inside the bulk gap while the Dirac points at the M points are very close to the valence or conduction band edges. Later, we will show this feature has important consequences for the electronic structures and band topology of (111) thin films.

In a thin film, the top and bottom surface states hybridize to open up energy gaps at these four Dirac points. It is important to treat films with an odd and even number of layers separately due to the difference in crystal symmetry: The former has inversion symmetry and the latter does not. Our calculations based on the tight-binding model of Lent *et al.* [35] show different band structures for the two cases, as shown in Fig. 1. Nonetheless, both are semiconductors with a small fundamental gap located at or near the Γ point, and a much larger band gap at M. This is because the penetration length of the surface states at M is much larger than the one at Γ, hence the hybridization-induced gap at M is correspondingly larger than the one at Γ by orders of magnitude. As a result of this inequivalence between Γ and M, (111) films of TCIs in the SnTe class are narrow-gap semiconductors, whose properties are controlled by low-energy physics at the Γ point.

To deduce the band topology, we build an effective $k \cdot p$ Hamiltonian at Γ. First considering the case of an even number of layers, here the top and bottom surfaces are different, terminated by Sn and Te atoms, respectively, which breaks the inversion symmetry (see the insets in Fig. 1). Each surface is described by a two-dimensional Dirac fermion, $H_{t,b} = v_{t,b}(k_x s_y - k_y s_x) + E_{t,b}$, where v_t and v_b denote the Dirac velocities of the top and bottom surfaces, respectively; E_t and E_b denote the Dirac point energies of the two surfaces. Denoting the two surfaces by $\tau_z = \pm 1$, the hybridization term to zeroth order in $\mathbf{k}$ is given by $m\tau_x$, which comes from the hybridization between the topological states on the top and bottom surfaces. This leads to a four-band $k \cdot p$ Hamiltonian

 ©2015 American Physical Society

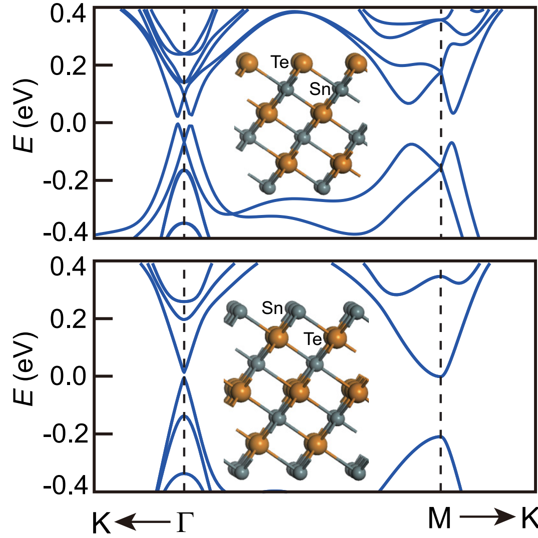

FIG. 1. (Color online) The typical band structures of (111) thin films: 24 layer (top) and 25 layer (bottom). The different symmetries of thin films with an even and odd number of layers (see insets) leads to their qualitatively different band structures.

for the film,

$$H(\mathbf{k}) = v(k_x s_y - k_y s_x)\tau_z + \delta\tau_z + m\tau_x. \quad (1)$$

Here, for simplicity, we have assumed that $v_t = -v_b = v$: Including two velocities of different magnitudes will not change the conclusion of the band topology determined from (1). $\delta = (E_t - E_b)/2$ measures the energy difference of the Dirac points at the top and bottom surfaces, which can be affected by a perpendicular electric field.

By diagonalizing the $H(\mathbf{k})$, we obtain four bands with energy-momentum dispersion $E_V(\mathbf{k})$, $E_W(\mathbf{k})$, $-E_V(\mathbf{k})$, and $-E_W(\mathbf{k})$, where $E_{V,W}(\mathbf{k})$ are given by

$$E_{V,W}(\mathbf{k}) = \sqrt{m^2 + \left[\sqrt{(k_x^2 + k_y^2)v^2} \pm \delta\right]^2}. \quad (2)$$

The δ term causes the two degenerate Dirac cones to split in energy. For $m = 0$, the hole band of the higher Dirac cone and the electron band of the lower Dirac cone will cross each other at $E = 0$, forming a circular Fermi surface defined by $(k_x^2 + k_y^2)v^2 = \delta^2$. Now, turning on the hybridization term $m \neq 0$ will open a gap at this circular Fermi surface, $E_g = 2|m|$. In addition, the gap at the Γ point increases to $E_g(\Gamma) = 2\sqrt{m^2 + \delta^2}$. The resulting band structure is particle-hole symmetric and has a Mexican hat dispersion, with degenerate band gaps around a circle in $\mathbf{k}$ space. This is indeed found in our band structure calculation, shown in the top panel of Fig. 1.

Importantly, the band structure (2) shows that the band gap does not close when δ is tuned to zero, as long as m stays finite. Therefore, the Z_2 topology can be determined by setting $\delta = 0$, and is controlled entirely by m, the coupling between the top and bottom surfaces. The Hamiltonian for $\delta = 0$ takes the form of a two-dimensional massive Dirac Hamiltonian, as in the Bernvig-Hughes-Zhang model for HgTe/CdTe quantum wells [24]. The sign of m controls the Z_2 topology. Similar to

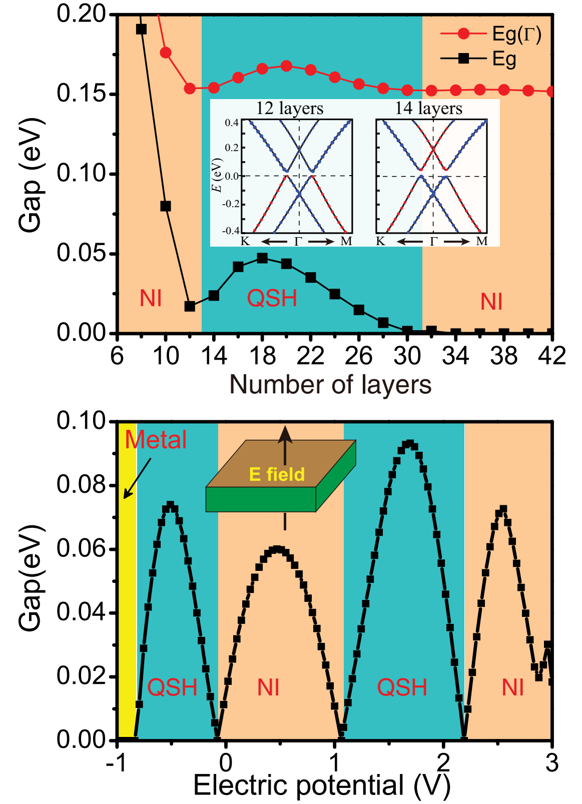

FIG. 2. (Color online) The effect of thickness (top) and the effect of external perpendicular electric field on a 12-layer thin film (bottom). The quantum spin Hall (QSH) phase can be achieved by changing the thickness or tuning the external electric field. The red (blue) dots in the inset of the top panel represent the states mainly composed of Te (Sn) atoms and the size means the corresponding weight.

previous proposals for Bi_2Se_3 thin films [26–28], we expect that the intersurface hybridization m, both its magnitude and sign, should depend on the film thickness, thereby leading to a gap change and a topological phase transition as a function of film thickness.

This is confirmed by our tight-binding calculations. As shown in the top panel of Fig. 2, both the fundamental gap E_g and the gap at the Γ point $E_g(\Gamma)$ change with the film thickness. When the thickness deceases, both gaps exhibit a oscillatory behavior, confirming our expectation from the above $k \cdot p$ model. The gap oscillation is expected to signal a sign change of the Dirac mass m, leading to Z_2 topological phase transitions between the 12- and 14-layer thin films. Furthermore, as shown in the inset of the top panel of Fig. 2, the conduction bands of the 12-layer thin film are mainly composed of Sn orbitals, while they are mainly from Te orbitals for the 14-layer thin film, suggesting that 12- and 14-layer thin films belong to different topological phases.

To determine which thickness range is topologically nontrivial, we directly calculate the edge states in a semi-infinite geometry by using the recursive Green's function method [36]. Without loss of generality, we take armchair-type edges as an example. As shown in Fig. 3, for a 14-layer thin film, the linear-dispersion gapless states exist in the bulk gap with a twofold

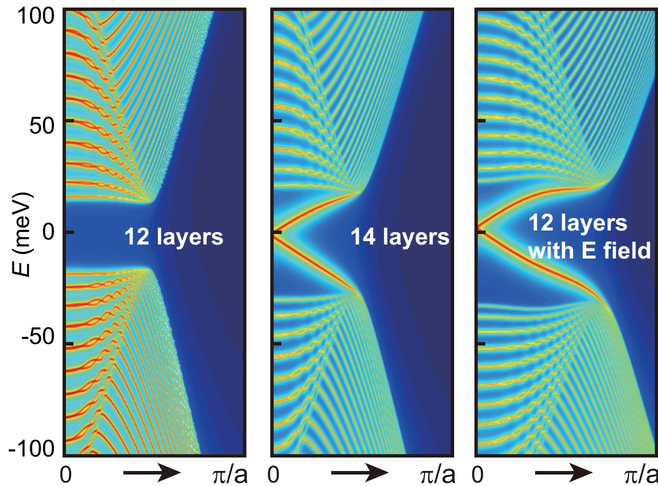

FIG. 3. (Color online) The edge states of a 12-layer thin film (left panel), 14-layer thin film (middle panel), and a 12-layer thin film under an electric field (right panel). For the 14-layer thin film, gapless states with a linear dispersion exist in the bulk gap, which confirm that the 14-layer thin film is in the quantum spin Hall (QSH) phase. Such kinds of edge states are absent for the 12-layer thin film, a normal insulator (NI), while we can drive a 12-layer thin film into the QSH phase by an external electric field. (The electric potential between the Te- and Sn-terminated surfaces is −0.2 V.)

degeneracy at the Γ point, called the Kramer's degeneracy, forming a one-dimensional Dirac point. In comparison, there are no such kinds of helical edge states in the 12-layer thin film. From such a calculation for other film thicknesses, we establish unambiguously a topological phase diagram shown in Fig. 2. In particular, all the thin films with an even number of layers between 14 and 30 layers are quantum spin Hall insulators.

In addition to its sensitivity to the thickness, we find that the intersurface coupling m can also be strongly affected by a perpendicular electric field [37]. Here the effect of an electric field is modeled by a linearly increasing electrostatic potential across the film thickness direction, leading to a potential difference ϕ between the Te- and Sn-terminated surfaces. We carefully calculate the evolution of the band structure of the 12-layer thin film by varying ϕ and find the gap exhibits an very interesting oscillated behavior: It indeed closes at some critical values, implying a topological phase transition induced by the electric field. Specifically, when we apply a negative electric field, the gap will first decrease and close at $\phi = -0.079$ V. As the electric field increases further, the gap reopens and achieves a maximum of around 75 meV at around $\phi = -0.51$ V and then goes down. If the electric field is strong enough, the thin film will become a metal. It is worth noting that the critical electric field strength for the topological phase transition is only around 4×10^7 V/m, which is an order smaller than the typical breakdown field strength for SnTe-related thin films [38]. To further verify this explicitly, we calculated the edge states for a 12-layer thin film under a different electric field. As shown in the Fig. 3, without an electric field, the edge states are fully gapped for the 12-layer thin film, while when the electric field is stronger than $\phi = -0.079$ V, there will be

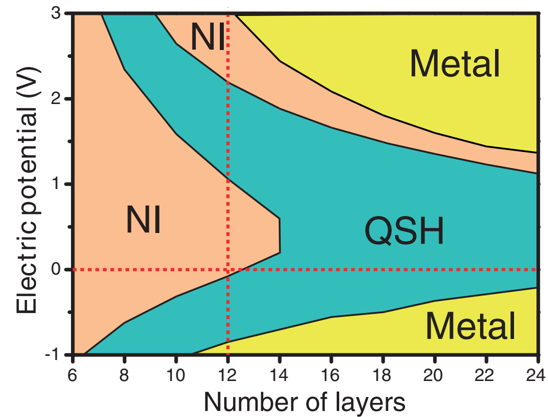

FIG. 4. (Color online) The phase diagram for thin films with an even number of layers varying with thickness and external electric field.

topologically protected edge states in the bulk gap (a typical result with $\phi = -0.2$ V is shown in the right panel). Similar behavior is seen at positive electric fields, with topological phase transitions at $\phi = 1.1$ and 2.2 V. The corresponding phase diagram is shown in Fig. 2.

By doing similar calculations for other film thicknesses, we obtain the complete phase diagram as a function of thickness and electric field, as shown in Fig. 4. From this we find that

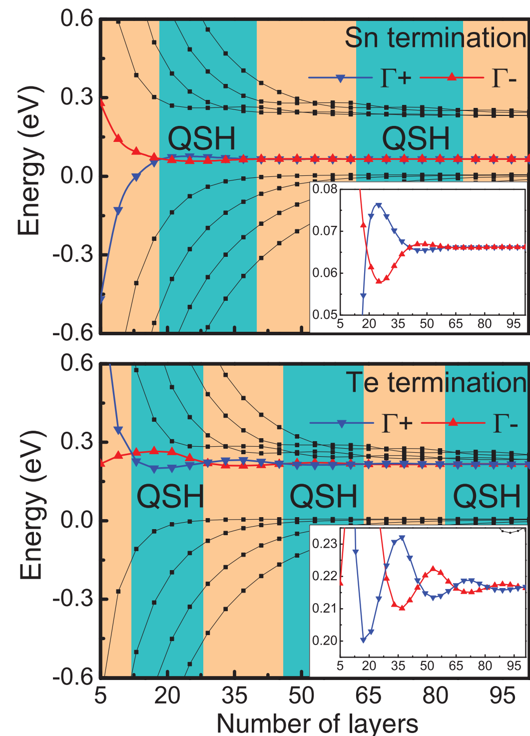

FIG. 5. (Color online) The subband energy level diagram at the Γ point and the topological phase diagram for (111) thin films with an odd number of layers with the Sn atom (top panel) and Te atom (bottom panel) terminated. The energy order of the Γ_+ and Γ_- states changes in oscillatory behavior with the number of layers, which results in a corresponding topological phase oscillation. The Dirac mass m (gap at the Γ point) is $m = E(\Gamma_+) - (\Gamma_-)$.

the quantum spin Hall phase of thin films thicker than 16 layers is very robust, whereas the thin films between 10 and 14 layers are very close to the phase boundary. Topological phase transitions can be realized under an experimentally feasible external electric field, which can be set up by using a top or bottom gate [37].

Now we turn to the case of thin films with an odd number of layers, where both surfaces are terminated by the same atoms (Sn or Te atoms) and inversion symmetry is present (see the insets in Fig. 1). The energy difference term $\delta\tau_z$ in the $k \cdot p$ Hamiltonian (1) is no longer allowed, leading to the standard Dirac Hamiltonian $H = m\sigma_x + v(k_x s_y - k_y s_x)\sigma_z$. The presence of inversion symmetry allows us to determine the topological invariant Z_2 based on the parity criterion [39]. Clearly, the conduction and valence bands at Γ are respectively the bonding and antibonding hybridizations of the top and bottom surface states, with opposite parities. Tight-binding calculations show that the 2D band structure near Γ is described very well by a single-valley Dirac fermion with a small mass, and the dispersion is linear and particle-hole symmetric in a sizable energy range (Fig. 1).

Figure 5 shows the energies of subbands at Γ for films thinner than 95 layers. The Dirac mass m, given by the energy difference between the bottom conduction and top valence band labeled as Γ_+ and Γ_-, depends nonmonotonously on the thickness. Importantly, m changes sign at certain critical thicknesses: 19, 39, 63, and 85 layers for Sn termination, and 13, 27, 47, 63, and 83 layers for Te termination. The Dirac mass reversal switches the parity of the conduction and valence band edges, resulting in a topological phase transition between a trivial insulator and a quantum spin Hall insulator. According to our tight-binding calculation, the band gap in the quantum spin Hall phase can reach 18 meV at 25 layers for Sn termination, and 66 meV at 19 layers for Te termination. The topological phase transition tuned by the film thickness is similar to the HgTe/CdTe quantum well [24]. Similar to thin films with an even number of layers, a perpendicular electric potential can also induce a topological phase transition for thin films with an odd number of layers.

The mechanism for realizing the quantum spin Hall phase in TCI thin films via intersurface coupling is similar to the thin films of topological insulators Bi_2Se_3 [26–28], which partly motivated this work. Due to the much larger penetration length of the SnTe surface states, the hybridization gap is much larger than that in Bi_2Se_3. Furthermore, the proposed quantum spin Hall phase in Bi_2Se_3 was found to depend very sensitively on the film thickness [26–28], with Z_2 topology changing back and forth with a period of only one or two quintuple layers. In comparison, our results show that the quantum spin Hall states in TCI films exist in an *extended* thickness range and hence are much more robust. Finally, our theoretical analysis of the electronic and topological properties of TCI thin films based on intersurface hybridization may apply to many other TCI materials that are currently being studied [40–44].

Note added. Recently, we learned of an independent work on (111) thin films of TCIs without an external electric field [45].

We thank Tim Hsieh for helpful discussions, and R. Buczko for alerting us to his work. This work was supported by the STC Center for Integrated Quantum Materials, NSF Grant No. DMR-1231319.

[1] L. Fu, Phys. Rev. Lett. **106**, 106802 (2011).
[2] Y. Ando and L. Fu, arXiv:1501.00531.
[3] T. H. Hsieh, H. Lin, J. Liu, W. Duan, A. Bansil, and L. Fu, Nat. Commun. **3**, 982 (2012).
[4] Y. Tanaka, Z. Ren, T. Sato, K. Nakayama, S. Souma, T. Takahashi, K. Segawa, and Y. Ando, Nat. Phys. **8**, 800 (2012).
[5] P. Dziawa, B. J. Kowalski, K. Dybko, R. Buczko, A. Szczerbakow, M. Szot, E. Łusakowska, T. Balasubramanian, B. M. Wojek, M. H. Berntsen, O. Tjernberg, and T. Story, Nat. Mater. **11**, 1023 (2012).
[6] S-Y. Xu, C. Liu, N. Alidoust, M. Neupane, D. Qian, I. Belopolski, J. D. Denlinger, Y. J. Wang, H. Lin, L. A. Wray, G. Landolt, B. Slomski, J. H. Dil, A. Marcinkova, E. Morosan, Q. Gibson, R. Sankar, F. C. Chou, R. J. Cava, A. Bansil, and M. Z. Hasan, Nat. Commun. **3**, 1192 (2012).
[7] Y. Okada, M. Serbyn, H. Lin, D. Walkup, W. Zhou, C. Dhital, M. Neupane, S. Xu, Y. Wang, R. Sankar, F. Chou, A. Bansil, M. Z. Hasan, S. D. Wilson, L. Fu, and V. Madhavan, Science **341**, 1496 (2013).
[8] I. Zeljkovic, Y. Okada, M. Serbyn, R. Sankar, D. Walkup, W. Zhou, J. Liu, G. Chang, Y. J. Wang, M. Z. Hasan, F. Chou, H. Lin, A. Bansil, L. Fu, and V. Madhavan, Nat. Mater. **14**, 318 (2015).
[9] M. Serbyn and L. Fu, Phys. Rev. B **90**, 035402 (2014).
[10] M. Safdar, Q. Wang, M. Mirza, Z. Wang, K. Xu, and J. He, Nano Lett. **13**, 5344 (2013).
[11] A. A. Taskin, F. Yang, S. Sasaki, K. Segawa, and Y. Ando, Phys. Rev. B **89**, 121302 (2014).
[12] J. Shen and J. J. Cha, Nanoscale **6**, 14133 (2014).
[13] J. Shen, Y. Jung, A. S. Disa, F. J. Walker, C. H. Ahn, and J. J. Cha, Nano Lett. **14**, 4183 (2014).
[14] H. Guo, C. H. Yan, J. Liu, Z. Y. Wang, R. Wu, Z. D. Zhang, L. L. Wang, K. He, X. C. Ma, S. H. Ji, W. Duan, X. Chen, and Q. K. Xue, APL Mater. **2**, 056106 (2014).
[15] C. Yan, J. Liu, Y. Zang, J. Wang, Z. Wang, P. Wang, Z. D. Zhang, L. Wang, X. C. Ma, S. Ji, K. He, L. Fu, W. Duan, Q. K. Xue, and X. Chen, Phys. Rev. Lett. **112**, 186801 (2014).
[16] B. A. Assaf, F. Katmis, P. Wei, B. Satpati, Z. Zhang, S. P. Bennett, V. G. Harris, J. S. Moodera, and D. Heiman, Appl. Phys. Lett. **105**, 102108 (2014).
[17] S. Sasaki and Y. Ando, arXiv:1410.4852.
[18] J. Liu, T. H. Hsieh, P. Wei, W. Duan, J. Moodera, and L. Fu, Nat. Mater. **13**, 178 (2014).
[19] R. Buczko and L. Cywinski, Phys. Rev. B **85**, 205319 (2012).
[20] X. Qian, L. Fu, and J. Li, Nano Res., doi:10.1007/s12274-014-0578-9 (2014).
[21] H. Ozawa, A. Yamakage, M. Sato, and Y. Tanaka, Phys. Rev. B **90**, 045309 (2014).
[22] M. Ezawa, New J. Phys. **16**, 065015 (2014).

[23] C. L. Kane and E. J. Mele, Phys. Rev. Lett. **95**, 226801 (2005); **95**, 146802 (2005).
[24] B. A. Bernevig, T. L. Hughes, and S. C. Zhang, Science **314**, 1757 (2006).
[25] M. König, S. Wiedmann, C. Brüne, A. Roth, H. Buhmann, L. W. Molenkamp, X.-L. Qi, and S.-C. Zhang, Science **318**, 766 (2007).
[26] J. Linder, T. Yokoyama, and A. Sudbø, Phys. Rev. B **80**, 205401 (2009).
[27] C. X. Liu, H. J. Zhang, B. Yan, X. L. Qi, T. Frauenheim, X. Dai, Z. Fang, and S. C. Zhang, Phys. Rev. B **81**, 041307 (2010).
[28] H.-Z. Lu, W.-Y. Shan, W. Yao, Q. Niu, and S.-Q. Shen, Phys. Rev. B **81**, 115407 (2010).
[29] J. Liu, W. Duan, and L. Fu, Phys. Rev. B **88**, 241303(R) (2013).
[30] J. Wang, J. Liu, Y. Xu, J. Wu, B. L. Gu, and W. Duan, Phys. Rev. B **89**, 125308 (2014).
[31] Y. J. Wang, W.-F. Tsai, H. Lin, S.-Y. Xu, M. Neupane, M. Z. Hasan, and A. Bansil, Phys. Rev. B **87**, 235317 (2013).
[32] S. Safaei, P. Kacman, and R. Buczko, Phys. Rev. B **88**, 045305 (2013).
[33] Y. Tanaka, T. Shoman, K. Nakayama, S. Souma, T. Sato, T. Takahashi, M. Novak, K. Segawa, and Y. Ando, Phys. Rev. B **88**, 235126 (2013).
[34] C. M. Polley, P. Dziawa, A. Reszka, A. Szczerbakow, R. Minikayev, J. Z. Domagala, S. Safaei, P. Kacman, R. Buczko, J. Adell, M. H. Berntsen, B. M. Wojek, O. Tjernberg, B. J. Kowalski, T. Story, and T. Balasubramanian, Phys. Rev. B **89**, 075317 (2014).
[35] C. S. Lent, M. A. Bowen, J. D. Dow, R. S. Allgaier, O. F. Sankey, and E. S. Ho, Superlattices Microstruct. **2**, 491 (1986).
[36] M. P. L. Sancho, J. M. L. Sancho, J. M. L. Sancho, and J. Rubio, J. Phys. F: Met. Phys. **15**, 851 (1985).
[37] X. Qian, J. Liu, L. Fu, and J. Li, Science **346**, 1344 (2014).
[38] S. Parvanov, V. Vassileva, and L. Aljihmania, J. Optoelectron. Adv. Mater. **7**, 1299 (2005).
[39] L. Fu and C. L. Kane, Phys. Rev. B **76**, 045302 (2007).
[40] M. Kargarian and G. A. Fiete, Phys. Rev. Lett. **110**, 156403 (2013).
[41] M. Kindermann, arXiv:1309.1667.
[42] M. Ye, J. W. Allen, and K. Sun, arXiv:1307.7191.
[43] H. Weng, J. Zhao, Z. Wang, Z. Fang, and X. Dai, Phys. Rev. Lett. **112**, 016403 (2014).
[44] T. H. Hsieh, J. Liu, and L. Fu, Phys. Rev. B **90**, 081112 (2014).
[45] S. Safaei, M. Galicka, P. Kacman, and R. Buczko, arXiv:1501.04728.